Investigation of the elution behavior of dissociating itaconic acid on a hydrophobic polymeric adsorbent using in-line Raman spectroscopy

Andreas Biselli[1], Alexander Echtermeyer[2], Rafael Reifsteck[1], Peter Materla[1], Alexander Mitsos[2,3,4], Jörn Viell[2], Andreas Jupke[1,*]

[1]Fluid Process Engineering (AVT.FVT), RWTH Aachen University, 52074 Aachen, Germany
[2]Process Systems Engineering (AVT.SVT), RWTH Aachen University, 52074 Aachen, Germany
[3]JARA-ENERGY, 52062 Aachen, Germany
[4]Energy Systems Engineering (IEK-10), Forschungszentrum Jülich, 52425 Jülich, Germany

Highlights:

- pH-dependent adsorption isotherms of itaconic acid on hydrophobic adsorbent
- pH-dependent pulse experiments of itaconic acid on hydrophobic adsorbent
- Raman spectroscopy for in-line measurements of acid species concentrations

This is the Authors' Accepted Manuscript of the following article: A. Biselli, A. Echtermeyer, R. Reifsteck, P. Materla, A. Mitsos, J. Viell, & A. Jupke (2022). Investigation of the elution behavior of dissociating itaconic acid on a hydrophobic polymeric adsorbent using in-line Raman spectroscopy. Journal of Chromatography A, 463140, which has been published in final form at: https://doi.org/10.1016/j.chroma.2022.463140.

Corresponding author: *A. Jupke
AVT Fluid Process Engineering, RWTH Aachen University, Forckenbeckstr. 51, 52074 Aachen, Germany
Phone: +49 241 80 95490, E-mail: andreas.jupke@avt.rwth-aachen.de

Abstract

The use of adsorption for the purification of dicarboxylic acids is rather limited and currently predominantly confined to ion-exchange chromatography. A promising, but less regarded alternative is the use of hydrophobic adsorbents. Regarding hydrophobic absorbents, the literature focuses on screenings of adsorbents for purification of (di)carboxylic acids with regard to adsorption equilibria. The investigation of dynamic phenomena in the column received only minor attention. In this contribution, this knowledge gap is addressed. First, the adsorption behavior of itaconic acid species on the hydrophobic, highly-crosslinked polymeric adsorbent Chromalite^{TM} PCG1200C is investigated. For this purpose, adsorption isotherms are determined via frontal analysis at pH values of 2, 3, 4.5, 6.5, and 8 to evaluate the dependency of the adsorption capacity on the dissociation state. Capacities above 150 g L_{ads}^{-1} at liquid phase concentrations of 70 g L^{-1} are observed at a pH of 2. A strong decrease of capacity with increasing pH value, i.e., with increasing fraction of dissociated negatively charged acid species, is observed. Second, pulse experiments at aforementioned pH values are performed. Thereby, in-line Raman spectra are recorded at the column outlet, which allows the direct differentiation of the acid species state of dissociation. The spectral information is evaluated for quantitative concentration profiles of itaconic acid species using Indirect Hard Modeling with mixture hard models that are calibrated subject to ideal as well as non-ideal thermodynamics. In-line measurement errors of ≤ 3.5 g L^{-1} are achieved for the itaconic acid species. In dependency of the pH of the feed solution, a separation of the individual acid species within the pulse experiments is observed. It is conjectured that the process is dominated by a superposition of species-dependent adsorption characteristics and dissociation reactions.

Keywords: Dicarboxylic acid, Raman spectroscopy, Species adsorption, Hydrophobic adsorbent, Process analytical technology

1 Introduction

For cost- and energy efficient purification of (di)carboxylic acids from fermentation supernatants, selective separation techniques with limited associated waste problems and low-energy requirements are necessary [1]. To date, many approaches for the purification of (di)carboxylic acids are reported in literature [2–5]. Thereby, adsorption processes have received some attention, with a focus on ion-exchange chromatography [6–8], a separation process which requires high amounts of salt solutions for the elution. The potential of non-ionic, hydrophobic adsorbents for the purification of (di)carboxylic acids, which may be operated with volatile organic solvents or even water for elution, thus decreasing waste streams, has only been investigated in a few studies. Efe *et al.* (2010) [9] evaluated the adsorption of succinic acid from aqueous solutions on powder zeolites, observing that the adsorption capacity depends substantially on the pH. They showed that the adsorption capacity decreases with increasing amount of dissociated species of succinic acid. Davison *et al.* (2020) [10] screened more than 25 adsorbents with regard to the adsorption of succinic acid from aqueous solutions, showing high capacities on hydrophobic molecular sieves. Schute *et al.* (2016) [11] investigated the potential of hydrophobic hyper-crosslinked polymers and certain low functionalized activated carbons for the purification of itaconic acid (IA). They performed an adsorbent screening for the identification of key adsorbent parameters for high IA capacity and identified high specific surface areas combined with highly hydrophobic surfaces of adsorbents as most relevant. Further, they showed high selectivities for IA adsorption against glucose, especially at low pH values, at which the fully protonated IA species is dominantly present.

However, besides first continuous adsorption and desorption experiments using a fixed bed column [11], previous research focused predominantly on adsorbent screenings evaluating the equilibrium thermodynamics. Thus, there is still a lack of knowledge with regard to the evaluation and mechanistic understanding of dynamic separation phenomena, such as acid species dependent adsorption and dissociation reactions within the fixed

bed column, necessary for a reliable design of the separation process.

To be able to observe a separation process in a time-resolved and direct manner, in-line process monitoring techniques can be applied. Some techniques are widely used in-line, in particular refractive index and pH measurements due to low expense and simple implementation. However, refractive index and pH measurements provide lumped signals that do not resolve concentration information of the chemical species in a complex mixture as required for understanding and improvement of the separation process. In contrast, spectroscopic monitoring techniques, such as in-line Raman spectroscopy, offer the opportunity to resolve the molecular structure, chemical interactions, and concentrations in particular of organic components dissolved in water [12]. Further, Raman spectroscopy can be used to differentiate in-line between different dissociation states of mineral and carboxylic acid species on a direct, time-resolved, and non-invasive basis [13–18].

However, to date, Raman spectroscopy for in-line monitoring of chromatographic processes found only application in some studies [19,20]. Here, Feidl *et al.* [20] demonstrated the feasibility of non-contact Raman optics for on-line detection of monoclonal antibodies in the eluate stream after protein A chromatography.

In this contribution, phenomena in the fixed bed column originating from the adsorption of the individual IA species IAH_2, IAH^-, and IA^{2-} (cf. Figure 2) from aqueous solution on a hydrophobic polymeric adsorbent are investigated. Thereby, in-line Raman spectroscopy using an immersion optic is employed to measure the concentrations of the individual IA species at the column outlet, thus increasing process understanding and offering the possibility for a reliable process design. First, adsorption isotherms are determined twofold via frontal analysis at pH values of 2, 3, 4.5, 6.5, and 8. The pH values are chosen to allow the allocation of the contribution of the individual acid species to the overall adsorption capacity. Second, pulse experiments are performed at aforementioned pH values, employing in-line Raman spectroscopy to measure the individual acid species at the column outlet. The recorded in-line Raman spectra are evaluated with

a chemometric method to translate the spectral data into quantitative compositional data [21, 22]. For this, we use and adapt our recent framework based on Indirect Hard Modeling (IHM) [23, 24]. Due to physically justified spectral Hard Models (HMs) for representation of the peaks of single chemical species in the mixture, IHM allows the deconvolution of strongly overlapping Raman peaks exhibited by the structurally similar dissociating IA species. This allows for differentiation and quantification of the IA dissociation states. Moreover, due to the flexible nature of the spectral HMs, IHM enables the compensation of nonlinear spectral effects such as peak shifts and deformations often occurring in electrolyte media, which would corrupt linear chemometrics such as peak integration or standard partial least squares regression [24–26]. To address the fact that at the investigated process conditions, the assumption of ideal thermodynamics regarding the thermodynamics of acid species dissociation may not hold due to high ionic strengths, two different mixture HMs are constructed to evaluate the spectral data [27, 28].

2 Materials and methods

2.1 Chemicals

IA and acetone, each with a purity of ≥99 % are purchased from VWR (Radnor, Pennsylvania, USA). Hydrochloric acid (HCl, 1N) and sodium hydroxide (NaOH, 20 wt% and 50 wt%) are purchased from Carl Roth & Co. KG (Karlsruhe, Germany). The adsorbent Chromalite™ PCG1200C is purchased from Purolite Ltd. (Ratingen, Germany). According to the manufacturer, the highly hydrophobic, polystyrenic, macroporous adsorbent has no functional group, a surface area (min.) of 600 m^2 g^{-1}, a typical porosity of 300 - 500 Å, and a particle size (80% in range) between 100 – 200 µm with a mean diameter of 125 – 175 µm [29]. For all experiments water is used, which is first deionized (< 0.7 µS cm^{-1}) and subsequently distilled.

2.2 Chromatography setup

Adsorption experiments are performed with an AZURA® LC system from Knauer Wissenschaftliche Geräte GmbH (Berlin, Germany) with P 6.1L and P 4.1S pumps. The setup is equipped with two in-line detectors for measurements of the refractive index. The analytical refractive index detector RID 2.1L (Knauer Wissenschaftliche Geräte GmbH) is used for the detection of tracer substances. The refractive index detector Abbemat 550 (Anton Paar, Graz, Austria) is used for in-line concentration measurements in breakthrough experiments. Further, a custom-made flow cell (cf. SI Figure S5) for the implementation of in-line Raman spectroscopy is added to the setup, adapted from our recent study [30]. For sample collection, the setup is equipped with a fraction collector. The dead volume of the setup is determined to approximately 4 mL. The investigated adsorbent is packed into a glass column of the type Supercompact with a length of 300 mm and an inner diameter of 16 mm, purchased from Götec Labortechnik GmbH (Bickenbach, Germany). The column has a double jacket and is tempered with water to 298.15 K.

Prior to packing of the column, the adsorbent is stirred in a beaker filled with acetone on a magnetic stirring plate for at least 30 min to ensure wetting of the pores. Afterwards, acetone is removed by replacing the liquid supernatant with water. The column is packed utilizing the slurry method [31]. The packed column is washed with at least 20 column volumes of water to remove remaining acetone. The final bed height has a value of 18.1 cm.

Tracer experiments are performed at a flow rate of 2 mL min^{-1} for evaluation of the packing quality as well as for determination of the total column porosity ε_t, using 1 mol L^{-1} sodium chloride and a 100 µL sample loop. The total column porosity is determined to 0.779.

2.3 Adsorption isotherm determination

Adsorption isotherms are determined twofold via frontal analysis [31]. Concentrations of IA up to 70 g L^{-1} at pH values adjusted with HCl or NaOH to 2, 3, 4.5, 6.5, and 8 are evaluated. The concentration at the column outlet is tracked in-line using the refractive index detector Abbemat 550 (Anton Paar, Graz, Austria). A pH-dependent calibration of the refractive index detector is performed based on the equilibrium stages of respective breakthrough curves. Concentrations of each breakthrough curve are validated by fractionation and subsequent HPLC analysis of gathered fractions. Adsorption isotherms are calculated based on breakthrough curves determined via the refractive index measurements due to higher data density.

All adsorption isotherms are fitted in Matlab R2021a (Mathworks, Massachusetts, USA) to mathematical models using the solver *lsqcurvefit*. Models are selected with respect to maximum coefficients of determination R^2. For all fittings, varying initial and boundary values yield the same isotherm parameter values, suggesting an optimal fit.

The isotherms for the pH values of 2 and 3 are fitted using the Redlich-Peterson model [32]

$$q_i = K_i \frac{c_{\mathrm{p},i}}{1 + b_i \cdot c_{\mathrm{p},i}^{g_i}}.$$

The isotherm for the pH value of 4.5 is fitted using the Freundlich model [33]

$$q_i = a_i \cdot c_{\mathrm{p},i}^{1/n_i}.$$

The isotherms for the pH values of 6.5 and 8 are fitted using the Henry model [31]

$$q_i = H_i \cdot c_{\mathrm{p},i}.$$

In all isotherm models, q_i represents the loading of the adsorbent with regard to ε_t in

g $L^{-1}_{\text{adsorbent}}$ and $c_{\text{p},i}$ the concentration of IA in the pore volume in g L^{-1}.

The parameters K_i, b_i and g_i, the parameters a_i and n_i, as well as the Henry coefficient H constitute fitting parameters [31–33].

2.4 pH-dependent pulse experiments

Pulse experiments are performed at aforementioned pH values in the feed solution of 2, 3, 4.5, 6.5, and 8. The IA concentrations in the feed vary due to adjustments of the pH values via HCl and NaOH and constitute final values of 66.2 g L^{-1}, 65.7 g L^{-1}, 61.3 g L^{-1}, 63.6 g L^{-1}, and 63.1 g L^{-1}, respectively. Prior to each pulse experiment, the column is rinsed with at least 15 column volumes of water. The experiments are performed with a volume flow rate of 2 mL min^{-1}. At the beginning of each experiment, 20 mL (10 min) of respective IA solution are injected to the column. Afterwards, water is injected in the column with identical flow rate for more than 90 min. The concentrations of the three IA species IAH_2, IAH^-, and IA^{2-} are determined via in-line Raman spectroscopy. Furthermore, 77 fractions of 1 mL volume of each pulse experiment are collected at the column outlet and analyzed with regard to the total IA concentration via HPLC analytics. A subset of the fractions is evaluated at-line with regard to the pH value.

2.5 HPLC analytics

The quantification of fractions with regard to their IA concentrations is performed with an Agilent 1260 Infinity II device (Agilent Technologies, Inc., Santa Clara, USA) utilizing the refractive index detector G7162A for sample quantification. An “Organic Acid Resin” column with a length of 100 mm and a diameter of 4.6 mm (CS-Chromatographie, Langerwehe, Germany) is used. The column is tempered to 303.15 K. 5 µL of respective samples are injected into an isocratic flow of 1 mL min^{-1} of 2.5 mM sulphuric acid.

2.6 pH measurements

The pH electrode InLab Routine Pro-ISM connected to the pH meter SevenCompact S220 is used for pH measurements (Mettler Toledo, Gießen, Germany). For at-line determination of pH values of fractionated samples in vials, the InLab Micro electrode (Mettler Toledo, Gießen, Germany) is used. A four-point calibration of the electrodes is performed on a daily basis utilizing buffers at the pH values of 2, 4, 7, and 10 (CHEMSOLUTE, Th. Geyer GmbH & Co. KG., Germany).

2.7 In-line Raman spectroscopy

A Raman spectrometer of the type RXN1 with a 400 mW laser at 785 nm from Kaiser Optical Systems (Ann Arbor, MI, USA) is used. The spectrometer is coupled with a 5 m fiber-optical cable and a near-infrared (NIR) immersion probe with sapphire optical window at a fixed focal distance of 0 mm (Kaiser Optical Systems, Ann Arbor, MI, USA) [34]. The immersion probe is fixed in a custom-made flow cell (cf. SI Figure S5), similar to another construction recently published by some of the authors [30]. The Raman spectrometer is controlled via the software iC Raman 4.1 (Kaiser Optical Systems, Ann Arbor, MI, USA). The recorded spectral range comprises $\tilde{\nu}$ = 160 – 3285 cm^{-1} at a spectral resolution of 4 cm^{-1}. Prior to each experiment, the focus of the instrument is set by adjustment of the Pixel-Fill to 55 %, which denotes the percentage of the Raman detector saturation. Measurements are performed every 45 s, utilizing an exposure time of 15 s with two repetition measurements per data point.

For calibration of the IHM, 57 spectra are used. 11 spectra are recorded at a constant flow rate of 2 mL min^{-1} through the custom-made flow cell for each of the pH values of 2, 3, 4.5, 6.5, and 8. Thereby, the concentrations of the respective 11 spectra are measured in equidistant steps between approximately 5 g L^{-1} and approximately 70 g L^{-1}. Further, a spectrum comprising signals of water and polytetrafluoroethylene (PTFE) from the wall of the flow cell, and a spectrum only comprising PTFE signals, recorded in the empty

and dry flow cell, are used.

pH-dependent IA species distribution

The reactions (1) – (5) are assumed to take place in the aqueous phase.

$$\mathrm{IAH_2} + \mathrm{H_2O} \overset{K_{\mathrm{a},1}}{\rightleftarrows} \mathrm{IAH^-} + \mathrm{H_3O^+} \tag{1}$$

$$\mathrm{IAH^-} + \mathrm{H_2O} \overset{K_{\mathrm{a},2}}{\rightleftarrows} \mathrm{IA^{2-}} + \mathrm{H_3O^+} \tag{2}$$

$$\mathrm{H_2O} + \mathrm{H_2O} \overset{K_{\mathrm{H_2O}}}{\rightleftarrows} \mathrm{H_3O^+} + \mathrm{OH^-} \tag{3}$$

$$\mathrm{HCl} + \mathrm{H_2O} \overset{K_{\mathrm{HCl}}}{\rightleftarrows} \mathrm{Cl^-} + \mathrm{H_3O^+} \tag{4}$$

$$\mathrm{NaOH} \overset{K_{\mathrm{NaOH}}}{\rightleftarrows} \mathrm{Na^+} + \mathrm{OH^-} \tag{5}$$

The calibration of the chemometrics on the basis of IHM requires the knowledge of the amount of $\mathrm{IAH_2}$, $\mathrm{IAH^-}$, $\mathrm{IA^{2-}}$, and $\mathrm{H_2O}$ in all calibration spectra. A natural representation of the necessary model would be a (high-index) differential-algebraic equation system [35, 36]. For historical reasons and consistency with our other simulation models, the dynamics are approximated via a system of ordinary differential equations [37] (cf. SI Equation System). This is solved in Matlab R2021a (Mathworks, Massachusetts, USA) using the solver *ode15s*. Thereby, $\mathrm{p}K_\mathrm{a}$ values of IA are assumed as $\mathrm{p}K_{\mathrm{a},1} = 3.84$ and $\mathrm{p}K_{\mathrm{a},2} = 5.45$ [38], whereas $\mathrm{p}K_\mathrm{w}$ is set to the standard value of 14. HCl and NaOH are assumed to fully dissociate by setting the K_{HCl} and K_{NaOH} values to 10^7, an arbitrary but sufficiently large value to ensure complete dissociation.

To investigate the effect of high ionic strength on IA dissociation, the acid species calculation is performed assuming either ideal thermodynamics or non-ideal thermodynamics. In the former case, activity coefficients γ_i of all components are by definition set to 1. For the case of non-ideal thermodynamics, γ_i of ionic components $i \in [\mathrm{IAH^-}, \mathrm{IA^{2-}}, \mathrm{H_3O^+}, \mathrm{OH^-}, \mathrm{Cl^-}, \mathrm{Na^+}]$ are calculated using the Truesdell and Jones

(TdJ) equation [39]

$$\log \gamma_i = -\frac{\mathrm{A} \cdot z_i^2 \cdot \sqrt{I}}{1 + \mathrm{B} \cdot \mathrm{a}_i \cdot \sqrt{I}} + \mathrm{b}_i \cdot I,$$

which has a reported validity up to ionic strengths of 2 mol L^{-1} [40].

For a temperature of 298.15 K, the parameters A and B have values of $A = 0.5116\ \mathrm{L}^{1/2}\mathrm{mol}^{-1/2}$ and $B = 0.3292\ \mathrm{L}^{1/2} \cdot 10^8 \mathrm{cm\ mol}^{-1/2}$ [41]. The variable I constitutes the ionic strength and is calculated according to

$$I = 0.5 \cdot \sum_i c_i \cdot z_i^2.$$

The variable z_i constitutes the charge of component i, and a_i and b_i represent fitting parameters [42]. According to common practice [28], γ_i of the uncharged components $i \in [\mathrm{IAH_2}, \mathrm{H_2O}, \mathrm{NaOH}, \mathrm{HCl}]$ are assumed as 1. The parameters a_i and b_i of the two ionic IA species IAH^- and IA^{2-} are determined in this work. For this, equilibrium states are fitted in Matlab R2021a (Mathworks, Massachusetts, USA) to experimentally determined titration curves utilizing the aforementioned set of equations and the solver *lsqcurvefit*.

Fitted values of a_i and b_i of the two ionic IA species IAH^- and IA^{2-} vary in dependency of used initial values within the fitting. Utilized values are chosen with respect to a significantly reduced sum of squared residuals (SSR)

$$SSR = \sum_{i=1}^{n} \left(\mathrm{pH}_{\mathrm{exp},i} - \mathrm{pH}_{\mathrm{sim},i}\right)^2 \tag{6}$$

compared to a calculation assuming ideal thermodynamics (cf. Figure 1).

Values for the other ions for the TdJ equation are available in literature [42] and are listed in Table 1.

Table 1: Parameters for the TdJ activity-model [42].

Ion	a_i	b_i
OH^-	10.65	0.21
H_3O^+	4.78	0.24
Cl^-	3.71	0.01
Na^+	4.32	0.06

Experimental titration curves of IA are determined twofold at constant IA concentrations of 30 g L^{-1}, 50 g L^{-1}, and 70 g L^{-1}. Respective solutions are filled in beakers located in a water bath. The water bath is located on a heated magnetic stirrer plate (RCT digital, IKA, Staufen, Germany). The temperature of the IA solutions is controlled at 298.15 K using a PT100 sensor connected to the heated magnetic stirrer plate. Sodium hydroxide solutions with IA concentrations of 30 g L^{-1}, 50 g L^{-1}, and 70 g L^{-1}, respectively, are used as titration reagents. After each titration step, the pH value is measured using the pH electrode InLab Routine Pro-ISM connected to the pH meter SevenCompact S220 (Mettler Toledo, Gießen, Germany).

Development of IHM

To translate the spectral data into concentration information, IHM is used. In contrast to other chemometric methods such as simple peak integration (PI) or advanced approaches employing partial least squares regessions (PLS), physically justified IHM can deal with spectra of highly overlapping species signals, accounts for nonlinear peak shifts and peak deformations, and can be calibrated subject to a closure constraint that supports robust and physically sound results [22, 24–26, 43].

Calculated compositions on a sodium-free basis for both evaluated activity models of the 57 calibration spectra are combined with the corresponding in-line Raman spectra to form two calibration data sets for the chemometric method of IHM. Together with these

two data sets, a spectrum comprising signals of water and PTFE from the adapter wall, and a spectrum only comprising PTFE signals as recorded in the empty, dry adapter are processed to prepare the IHM method.

Following our recent contribution [23], Raman spectra comprising signals of only two liquid components, namely water and one IA species, as well as signals of PTFE, are determined or calculated from the calibration data set. Spectra comprising only Raman bands of water, IAH_2, and PTFE as well as Raman bands of water, IA^{2-}, and PTFE, respectively, are directly accessible from the calibration experiments at lowest and highest pH values. To prepare a spectrum only comprising Raman bands of water, IAH^-, and PTFE, the two aforementioned spectra are subtracted from the Raman spectrum corresponding to the experiment with the highest content of IAH^- species while weighted with the respective content of the acid species IAH_2 and IA^{2-} [23].

The subtraction is done for both calibration data sets in Matlab ver. 2018b employing GSTools ver. 0.4.2 for exchange of Raman spectra with Matlab and mdatools ver. 0.1.6 for SNV normalization prior to spectra subtraction [23,44–46]. A spectral range of 1025 – 1850 cm^{-1} with an excluded range of 1545 – 1565 cm^{-1} to erase signals of atmospheric oxygen in the pathway of the laser beam is applied [34, 47].

Using PEAXACT ver. 5.3 – 5.4 (S-PACT, Aachen, Germany), pure component models (PCMs) of each IA species, water, and PTFE are constructed on the basis of the two-component spectra, the water-PTFE spectrum, and the spectrum comprising the PTFE signals of the dry adapter wall [25, 48].

In a first step, a PCM of PTFE is constructed by fitting eight pseudo-Voigt profiles to the Raman spectrum of the dry adapter wall exhibiting only PTFE Raman bands. In a second step, the PCM of PTFE is used for Complemental Hard Modeling (CHM) to build a PCM of water with three pseudo-Voigt profiles [49]. Both, the PCM of PTFE and water are employed for contruction of PCMs for each IA species. Thereby, IAH_2 is modeled with seven, IAH^- with nine (for both calibration data sets), and IA^{2-} with nine

pseudo-Voigt profiles.

The PCMs are combined in two mixture hard models (HM) with a linear baseline of which each HM comprises the same PCMs of water, PTFE, IAH_2, and IA^{2-}, whereas they differ in the PCM of IAH^- subject to the underlying calculation basis that either considers non-ideality or not. For the HMs, no standardization model is included. With a total number of 12 free parameters (five component weights, five component shifts in a range of $\pm$ 10 cm^{-1}, and two baseline parameters), the mixture HMs are fitted in PEAXACT to the Raman spectra by adjustment of the free parameters. All other HM parameters are fixed and remain at the corresponding values determined during PCM construction.

Using PEAXACT, the mixture HM built on the basis of ideality assumptions for calculation of the calibration samples is subsequently calibrated employing the calibration data set comprising 55 in-line Raman spectra with corresponding composition data that is calculated subject to ideality assumptions. Analogously, the mixture HM built on the TdJ data set is calibrated with the same 55 in-line Raman spectra, however with underlying composition data considering non-ideal mixture behavior.

Both mixture HMs are calibrated subject to a closure constraint $\sum x_{k,j}^{\mathrm{aq}} = 1$ with $k \in [IAH_2, IAH^-, IA^{2-}, H_2O]$. The PCM of PTFE is not included in the closure constraint as it only serves as a "dummy" component for compensation of the PTFE Raman bands that overlap with the water and IA species Raman bands in the spectral range of evaluation.

For the calibration of both mixture HMs, random leave-10%-out cross-validations are performed [48]. The goodness of the calibrations is validated by evaluation of figures of merit such as the coefficient of determination R_k^2, the root mean square error of calibration $RMSEC_k$, the root mean square error of cross-validation $RMSECV_k$, and the limit of detection $LOD_k = \bar{x}_{k,\mathrm{blank}} + \beta\sigma_{k,\mathrm{blank}}$. For the latter, 27 blank measurements of water in the PTFE custom-made flow cell are recorded and evaluated. Thereby, $\bar{x}_{k,\mathrm{blank}}$ denotes the mean mole fraction, $\beta = 3.3$ the confidence factor equaling a confidence level of

95%, and $\sigma_{k,\text{blank}}$ the standard deviation of the evaluated blank measurements [50, 51].

3 Results and discussion

3.1 pH-dependent IA species distribution

Figure 1 depicts experimentally determined titration curves for IA concentrations of 30 g L^{-1}, 50 g L^{-1}, and 70 g L^{-1} and correspondingly calculated pH values assuming ideal thermodynamics (γ_i = 1) and non-ideal thermodynamics ($\gamma_i \neq 1$), utilizing the TdJ equation.

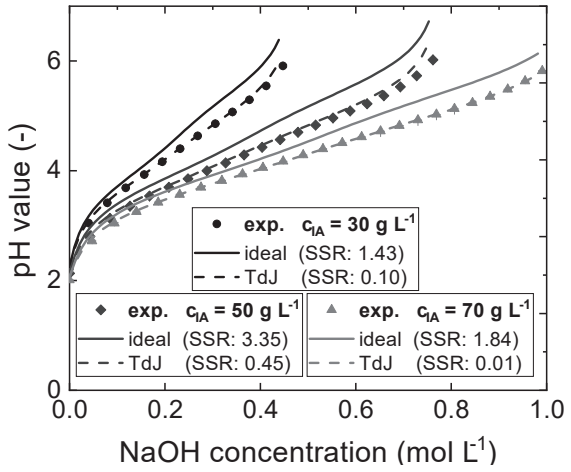

Figure 1: Prediction of the pH assuming ideal (γ_i = 1) and non-ideal thermodynamics (TdJ, $\gamma_i \neq 1$) compared to experimentally determined titration curves. The TdJ parameters a_i and b_i of the IA species IAH^- and IA^{2-} are fitted to the 70 g L^{-1} experimental titration curve.

Comparing experimentally determined titration curves and accordingly calculated pH values assuming ideal thermodynamics, deviations in terms of an overestimation of the calculated pH become apparent. It is assumed that deviations in the prediction of the pH are observed due to the invalid assumption of ideal thermodynamics. Therefore, the assumption of non-ideal thermodynamics is made. The TdJ parameters a_i and b_i of the two ionic IA species IAH^- and IA^{2-} are fitted to the 70 g L^{-1} titration curve. Thereby,

the parameters a_i and b_i yielded values of 0.023 and 0.47 for IAH^- and 4.45 and 0.4 for IA^{2-}, respectively. The parameters are validated with the 30 g L^{-1} and 50 g L^{-1} titration curves. Comparing the SSR of experimentally determined titration curves and accordingly calculated pH values assuming ideal and non-ideal thermodynamics, a remarkably reduced SSR is observed when utilizing the TdJ equation.

Figure 2 depicts calculated IA species distributions for pK_a values of 3.84 and 5.45 [38] for a IA concentrations of 70 g L^{-1} for the assumptions of ideal and non-ideal thermodynamics, utilizing the TdJ equation with aforementioned fitted TdJ parameters for IAH^- and IA^{2-}.

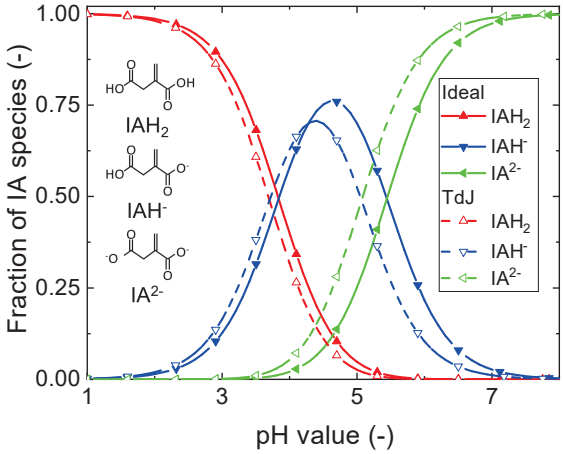

Figure 2: pH-dependent distribution of IAH_2, IAH^-, and IA^{2-} for ideal thermodynamics (γ_i = 1) and non-ideal thermodynamics (TdJ, $\gamma_i \neq 1$) for 70 g L^{-1} IA utilizing fitted parameters a_i and b_i of IAH^- and IA^{2-}.

At low pH values predominantly IAH_2 is present. With increasing pH, the fractions of IAH^- and IA^{2-} increase, whereby the fraction of IAH_2 continuously decreases. Utilizing the TdJ equation and aforementioned fitted TdJ parameters a_{IAH^-} and $a_{IA^{2-}}$ as well as b_{IAH^-} and $b_{IA^{2-}}$, the pH-dependent fractions of the species generally shift to lower pH values. Dependent on the pH, remarkable changes in the fractions of the three IA species are observed. Furthermore, the maximum fraction of IAH^- decreases.

3.2 pH-dependent adsorption isotherms of IA

In Figure 3, the pH-dependent adsorption isotherms of IA on the highly crosslinked, non-functionalized polymeric adsorbent Chromalite™ PCG1200C are depicted.

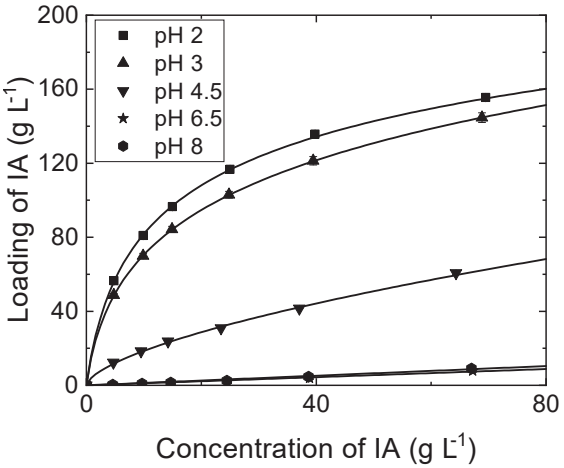

Figure 3: Experimentally determined pH-dependent adsorption isotherms of IA in aqueous solution on the highly crosslinked non-functionalized polymeric adsorbent Chromalite™ PCG1200C.

Table 2 lists associated adsorption isotherm parameters and respective coefficients of determination R^2 (cf. Section 2.3).

Table 2: Adsorption isotherm parameters for the pH values of 2, 3, 4.5, 6.5, and 8 and respective coefficients of determination R^2 (cf. Section 2.3).

isotherm	K	b	g	a	n	H	R^2
pH 2	23.46	0.27	0.84	-	-	-	0.99
pH 3	24.11	0.42	0.76	-	-	-	0.99
pH 4.5	-	-	-	4.41	1.60	-	0.99
pH 6.5	-	-	-	-	-	0.11	0.95
pH 8	-	-	-	-	-	0.13	0.98

The adsorption capacity of the hydrophobic polymeric adsorbent for IA is highest at low pH values and decreases with increasing pH. These observations are in agreement with results presented by Schute *et al.* [11]. For evaluation of the adsorption behavior of the individual IA species IAH_2, IAH^-, and IA^{2-}, the pH-dependent species distributions (cf. Figure 2) are taken into account. The highest adsorption capacity is observed at a pH of 2. At this pH, predominantly IAH_2 is present, indicating that IAH_2 adsorbs to the adsorbent surface. With increasing pH and thus increasing fraction of the dissociated species IAH^- and IA^{2-}, the adsorption capacity for IA decreases. At the pH values of 6.5 and 8, no IAH_2 is present. Corresponding Henry coefficients (cf. Table 2) of respective adsorption isotherms are similar and both very low. Since the evaluated activity models predict 8% (ideal) and 3.5% (TdJ) of IAH^- present at pH 6.5, it is assumed that both, IAH^- and IA^{2-}, only adsorb to a minor extent, due to their negative surface charge.

3.3 pH-dependent pulse experiments

As discussed in Section 3.2, it is concluded that in particular IAH_2 adsorbs to the adsorbent surface, whereas IAH^- and IA^{2-} adsorption is significantly less. To investigate dynamic phenomena within the separation column originating from IA species dependent adsorption and dissociation reactions, pH-dependent pulse experiments are conducted. Thereby, in-line Raman spectroscopy is employed for an in-line monitoring of the IA species IAH_2, IAH^-, and IA^{2-} at the column outlet. This approach allows an in-depth analysis of resulting chromatograms and offers the possibility to significantly increase the process understanding.

Figure 4 exemplarily depicts recorded Raman spectra at the column outlet of two pulse experiments at different feed pH values and thus varying species concentrations.

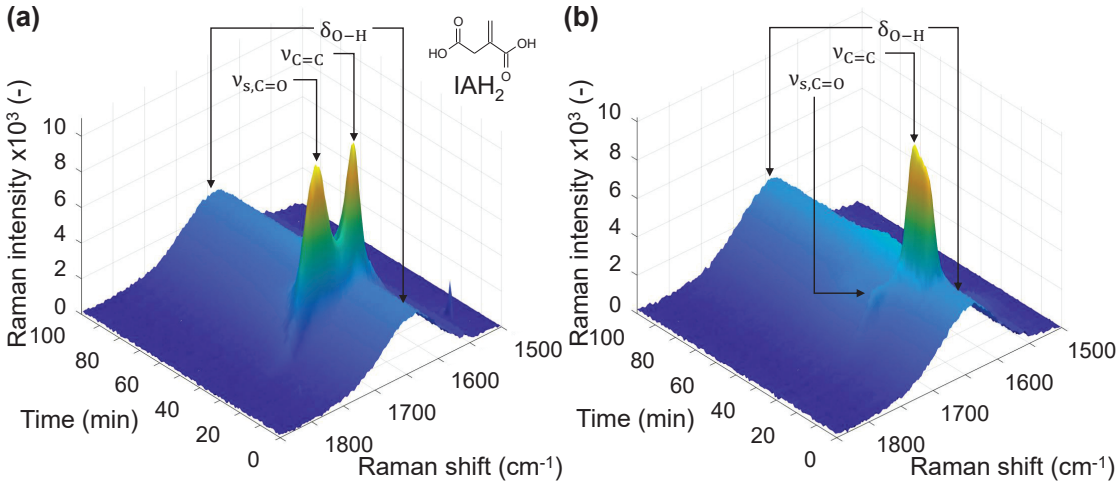

Figure 4: Raman spectra recorded at the column outlet of pulse experiments at pH values in the feed solutions of 2 (a) and 4.5 (b).

Only the spectral range of 1565 – 1850 cm^{-1} is shown as it represents the crucial region for the determination of individual IA species concentrations (cf. Section 2.7). Two characteristic peaks can be observed. The peak originating from the C=C double bond is present independently of the dissociation state of IA, whereas the peak C=O represents the amount of protonated carboxylic acid groups.

In Figure 4 (a) the Raman spectra of the pulse experiment with a pH of 2 in the feed solution are depicted. At a pH of 2, predominantly IAH_2 is present. Thus, two peaks are observed, which are caused by both aforementioned molecular bonds. Figure 4 (b) depicts recorded Raman spectra at a pH of 4.5 in the feed solution, at which the overall fractions of dissociated species are increased. Contrary to Figure 4 (a), the height of the C=O peak is significantly decreased, which is in accordance with Figure 2, since only 16.2% of IAH_2 and 75.2% of IAH^- (ideal) are present at a pH of 4.5.

Recorded Raman spectra of all pulse experiments are analyzed using presented HM (cf. Section 2.7) for quantitative Raman spectra analysis for the assumptions of ideal and non-ideal thermodynamics.

399 **HM calibration assuming ideal thermodynamics (γ_i = 1)**

400 Figures 5 (a) - (e) depict chromatograms of pulse experiments at pH values in the feed
401 solutions of 2, 3, 4.5, 6.5, and 8, respectively.

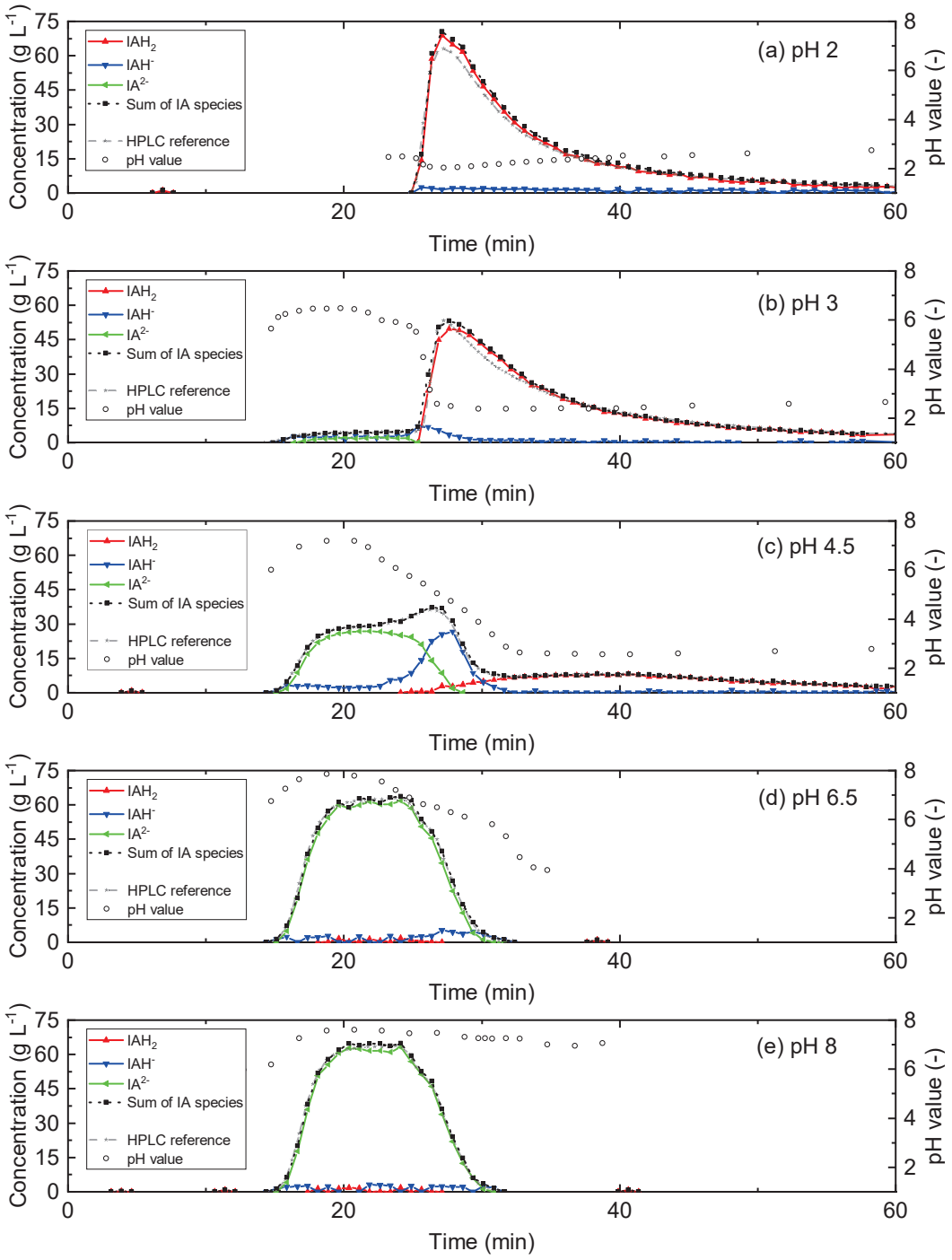

Figure 5: Pulse experiments at pH values in the feed solutions of 2 (a), 3 (b), 4.5 (c), 6.5 (d), and 8 (e). Chromatograms of the pulse experiments show IA species concentrations determined via in-line Raman spectroscopy, the total IA concentration as the sum of these species, the total IA concentration determined via HPLC analytics, as well as at-line pH value measurements during IA elution.

All chromatograms show the concentration courses of the IA species IAH_2, IAH^-, and IA^{2-} measured via in-line Raman spectroscopy, the total IA concentration as the sum of these species, at-line pH measurements, and total IA concentrations determined via HPLC analytics. For all pulse experiments, at-line pH measurements and total IA concentrations determined via HPLC analytics confirm measured species concentrations via in-line Raman spectroscopy. Further, the total IA concentrations determined via HPLC analytics and the total IA concentrations determined as the sum of species via in-line Raman spectroscopy are in very good agreement, thus proving the applicability of in-line Raman spectroscopy for (species) concentration determination of organic acids in chromatographic separation processes. Although not explicitly measured, we assume in consensus with the charge balance that locally high concentrations of dissociated IA also imply locally high sodium concentrations, ensuring electroneutrality.

Figure 5 (a) depicts the chromatogram of the pulse experiment at a pH of 2 in the feed solution, at which predominantly IAH_2 and minor fractions of IAH^- are present. The elution of IA starts at 25 min. The observed characteristic steep front along with a strong tailing is consistent for concave shaped isotherms (cf. Figure 3). The peak is composed particularly of IAH_2. Minor fractions of IAH^- are detected throughout the elution. These fractions are assumed to originate from dissociation reactions of IAH_2.

Figure 5 (b) depicts the chromatogramm of the pulse experiment at a pH of 3 in the feed solution. At a pH of 3, 87.2% of IAH_2 and 12.7% of IAH^- are present in the feed solution. The elution of IA starts at approx. 15 min at a low and almost constant concentration level of 4 g L^{-1} until approx. 26 min. This plateau originates from the elution of the negatively charged IA species IAH^- and IA^{2-}, which both adsorb only to a minor extent (cf. Section 3.2). Since the fraction of IA^{2-} at a pH of 3 is below 0.1%, fractions of IA^{2-} are assumed to originate from dissociation reactions of IAH^-. After approx. 26 min, a peak of IAH_2 with a characteristic steep front along with a strong tailing is observed, similarly to Figure 5 (a). The elution is again associated with minor

concentrations of IAH^- originating from dissociation reactions of IAH_2.

Figure 5 (c) depicts the chromatogram of the pulse experiment at a pH of 4.5 in the feed solution. At a pH of 4.5, all three IA species present in the feed solution are injected to the column (IAH_2 (16.2%), IAH^- (75.2%), and IA^{2-}(8.6%)). The chromatogram has a complex shape. In particular at this point, in-line Raman spectroscopy enables the in-depth analysis of the complex elution behavior by revealing the individual acid species within the chromatogram, thus significantly increasing the process understanding. It is shown that the complex chromatogram is caused by the superposition of three peaks, originating from the three IA species. IA^{2-} and minor concentrations of IAH^- elute from approx. 15 min. Thereby, the peak of IA^{2-} has a Gaussian shape, which is consistent for linear shaped isotherms or negligible adsorption. Since only 8.6% of IA^{2-} is present in the feed solution, the comparably large IA^{2-} peak is assumed to originate from dissociation reactions of IAH^-, which is validated via mass balance. Minor concentrations of IAH^- during the elution of IA^{2-} are observed. IAH^- elutes predominantly between 25 - 29 min. The delayed elution of IAH^- compared to IA^{2-} is assumed to originate from the continuous protonation of IAH^- and dissociation of IAH_2, leading to a retention of IAH^- due to the adsorption of IAH_2. This assumption is based on the fact that isotherms for pH 6.5 (8.0% IAH^-, 92.0% IA^{2-}) and pH 8 (0.2% IAH^-, 99.8% IA^{2-}) have comparable and only minor Henry coefficients. IAH_2 elutes from approx. 25 min, again showing a pronounced tailing.

Figures 5 (d) and (e) depict the chromatograms at pH values of 6.5 and 8 in the feed solutions, respectively. In both chromatograms, IA elution starts from approx. 15 min. Both peaks have a Gaussian shape, which is consistent with their linear shaped isotherms and the assumption of negligible adsorption (cf. Figure 3). Both peaks are predominantly composed of IA^{2-} and minor fractions of IAH^-. Low concentrations of IAH_2 are detected between 18 – 26 min. However, these concentrations are small and in the range of the detection limit (cf. SI Figure S8 (b)). Increased concentrations of IAH^- are detected at

a feed pH of 6.5 between approx. 26 – 30 min, due to 8.0% IAH^- in the feed solution.

HM calibration assuming non-ideal thermodynamics (TdJ, $\gamma_i \neq 1$)

To evaluate the influence of high ionic strengths on dissociation equilibria and thus on the Raman calibration, the TdJ equation (cf. Section 2.7) is applied for the calculation of activity coefficients. The calibration results for the mixture HM assuming non-ideal thermodynamics are depicted in Figure S4 in the SI and discussed in comparison to the results under the assumption of ideal thermodynamics. As expected, the calibration accuracy improves for the dissociated species IAH^- and IA^{2-}, showing a difference to the calibration performance of the ideal case $< 16\%$. Figure 6 exemplarily depicts the pulse experiment at a pH of 4.5 in the feed solution, which is evaluated employing the calibrated HM for quantitative Raman spectra analysis for the assumptions of ideal and non-ideal thermodynamics.

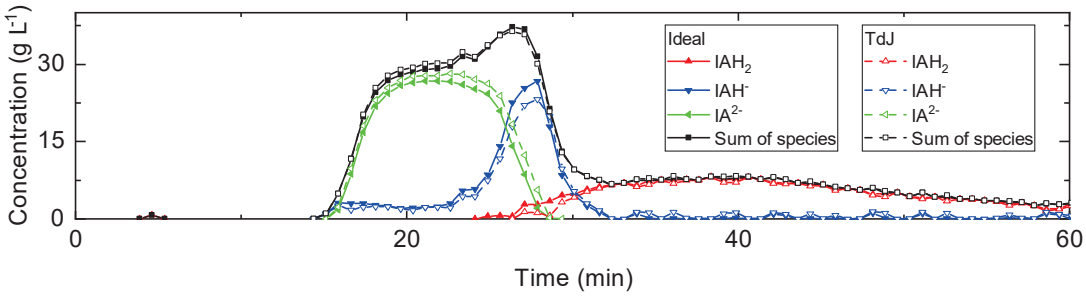

Figure 6: Pulse experiment at pH 4.5 in the feed solution. Comparison of species concentrations measured via in-line Raman spectroscopy and evaluated with HMs that are calibrated based on the assumptions of ideal and non-ideal thermodynamics.

The sum of IA species are in very good agreement for both cases. Comparing the peaks of the individual species, differences in the concentrations, in particular for IAH^- and IA^{2-} become apparent, which are in accordance with the observed shift in the species concentrations when assuming non-ideal thermodynamics (cf. Figure 2). Compared to the assumption of ideal thermodynamics, the assumption of non-ideal thermodynamics

leads to higher concentrations of IA^{2-} and lower concentrations of IAH^{-}. The concentrations of IAH_2 are not affected by the used activity coefficient model. The decision whether ideal or non-ideal thermodynamics are assumed for calibration of the chemometrics should be made dependent on the required accuracy in concentration measurements.

4 Conclusion

In this contribution, the adsorption behavior of IA species on a hydrophobic polymeric adsorbent is investigated. Adsorption isotherms show that the adsorption capacity for IA strongly increases with decreasing pH, which indicates that predominantly the fully protonated species IAH_2 adsorbs, whereas the adsorption of the negatively charged species IAH^{-} and IA^{2-} is negligible. Within pH-dependent pulse experiments utilizing in-line Raman spectroscopy for IA species measurements, a separation of the IA species is observed, which supports the aforementioned assumption that in particular IAH_2 adsorbs. Further, it leads to the conclusion that a retention of IAH^{-} takes place, which is based on the adsorption of IAH_2 and the dissociation of IAH_2 to IAH^{-}. It is concluded that the overall separation process is dominated by an interplay of the adsorption of IAH_2 and resulting dissociation reactions, since both, adsorption and dissociation reactions, strive for equilibrium. Calibrating the chemometrics for in-line Raman spectroscopy on the basis of IHM, the three acid species IAH_2, IAH^{-}, and IA^{2-} are successfully distinguished and quantified at the column outlet. The consideration of non-ideal thermodynamics to account for effects of high ionic strength on dissociation shows only a minor effect on IHM calibration accuracy. The additional complexity of considering non-ideal thermodynamics when calibrating chemometrics should be taken in dependency of the required accuracy of the measurements. While in this study only the concentrations of four components (IAH_2, IAH^{-}, IA^{2-}, H_2O) are tracked at the column outlet by in-line Raman spectroscopy, the presented approach may be extended to further Raman active components, such as glucose, for in-line process monitoring of chromatographic processes.

Further, the presented approach can be extended to the simultaneous in-line concentration measurement of multiple (di)carboxylic acids. However, 95% confidence intervals within this study show a limited significance for concentrations below approximately 3.5 g L^{-1}, which makes the quantitative measurement of low concentrated compounds unreliable. Presented results increase the fundamental understanding of dynamic phenomena in the separation column utilizing hydrophobic adsorbents originating from the presence and individual adsorption and dissociation characteristics of (di)carboxylic acid species. Therefore, our study contributes to a knowledge-based process design of associated separation tasks.

5 Acknowlegdements

The authors thank Janik Hense and Thomas Fuchs for proofreading the manuscript.

6 Conflict of interest

The authors declare that there is no conflict of interest.

7 Funding

A. Biselli, R. Reifsteck, and A. Jupke gratefully acknowledge the financial support by the Federal Ministry of Education and Research (BMBF) in the project BioSorp (FKZ 031B0678A) and the project supervision by the project management organization Projektträger Jülich (PtJ). A. Echtermeyer, A. Mitsos, and J. Viell gratefully acknowledge the financial support of the project ContiHighSolid (FKZ 031B0679) by the Federal Ministry of Education and Research (BMBF) and the project supervision by the project management organization Projektträger Jülich (PtJ).

8 Supplementary material

Contents of supplementary material include

- Equation system for calculation of compositional data.
- Visualization of pure component models and mixture hard models for all species, water, and PTFE for both used activity models.
- Parity plots and figures of merit for HM calibration of the three species and water for ideal and non-ideal (TdJ) thermodynamics.
- Schematic illustration and pictures of the custom-made flow cell.
- Exemplary results of the pulse experiments at feed pH values of 2, 4.5, and 8, including 95% uncertainties.

9 ORCID iD

Andreas Biselli: https://orcid.org/0000-0003-1498-1885
Alexander Echtermeyer: https://orcid.org/0000-0002-9382-2227
Rafael Reifsteck:
Peter Materla:
Alexander Mitsos: https://orcid.org/0000-0003-0335-6566
Jörn Viell: https://orcid.org/0000-0003-0587-6151
Andreas Jupke: http://orcid.org/0000-0001-6551-5695

10 Author contributions

- **A.B.**: Conceptualization of the research; Conduction of experimental work; Discussion and analysis of experimental results; Discussion and analysis of fitting results; Preparation of the manuscript; Reviewing and editing the manuscript.

- **A.E.**: Construction of PCMs and IHM; Calibration of IHM; Evaluation of spectral data with IHM; Discussion and analysis of measurement results; Preparation of the manuscript; Reviewing and editing the manuscript.
- **R.R.**: Processing and evaluation of experimental data; Conduction of fittings; Preparation of the manuscript.
- **P.M.**: Design of flow-through cell.
- **A.M.**: Scientific support, guidance, and discussion on methods and results; Advice on structure of publication; Reviewing and editing the manuscript.
- **J.V.**: Scientific support, guidance, and discussion on methods and results; Advice on structure of publication; Reviewing and editing the manuscript.
- **A.J.**: Design of the project, Scientific support, guidance, and discussion on methods and results; Advice on structure of publication; Reviewing and editing the manuscript.

References

[1] D. S. Sholl and R. P. Lively. Seven chemical separations to change the world. *Nature News*, 532(7600):435–437, 2016.

[2] A. I. Magalhães, J. C. de Carvalho, J. D. C. Medina, and C. R. Soccol. Downstream process development in biotechnological itaconic acid manufacturing. *Appl. Microbiol. Biotechnol.*, 101(1):1–12, 2017.

[3] M. Okabe, D. Lies, S. Kanamasa, and E. Y. Park. Biotechnological production of itaconic acid and its biosynthesis in *Aspergillus terreus*. *Appl. Microbiol. Biotechnol.*, 84(4):597–606, 2009.

564 [4] M. Gausmann, C. Kocks, M. Doeker, A. Eggert, T. Maßmann, and A. Jupke. Re-
565 covery of succinic acid by integrated multi-phase electrochemical pH-shift extraction
566 and crystallization. *Sep. Purif. Technol.*, 240(4):116489, 2020.

567 [5] C. Kocks, J. Görtz, A. Holtz, M. Gausmann, and A. Jupke. Electrochemical crystal-
568 lization concept for succinic acid reduces waste salt production. *Chem. Ing. Tech.*,
569 92(3):221–228, 2020.

570 [6] C. S. López-Garzón and A. J.J. Straathof. Recovery of carboxylic acids produced
571 by fermentation. *Biotechnol. Adv.*, 32(5):873–904, 2014.

572 [7] A. I. Magalhães, J. C. de Carvalho, E. N. M. Ramírez, J. D. C. Medina, and C. R.
573 Soccol. Separation of itaconic acid from aqueous solution onto ion-exchange resins.
574 *J. Chem. Eng. Data*, 61(1):430–437, 2016.

575 [8] A. I. Magalhães, J. C. de Carvalho, J. F. Thoms, J. D. C. Medina, and C. R. Soccol.
576 Techno-economic analysis of downstream processes in itaconic acid production from
577 fermentation broth. *J. Clean. Prod.*, 206:336–348, 2019.

578 [9] C. Efe, van der Wielen, L. A. M., and A. J. J. Straathof. High silica zeolites as an
579 alternative to weak base adsorbents in succinic acid recovery. *Ind. Eng. Chem. Res.*,
580 49(4):1837–1843, 2010.

581 [10] B. H. Davison, N. P. Nghiem, and G. L. Richardson. Succinic acid adsorption from
582 fermentation broth and regeneration. *Appl. Biochem. Biotechnol.*, 114(1-3):653–670,
583 2004.

584 [11] K. Schute, C. Detoni, A. Kann, O. Jung, R. Palkovits, and M. Rose. Separation in
585 biorefineries by liquid phase adsorption: Itaconic acid as case study. *ACS Sustain.*
586 *Chem. Eng.*, 4(11):5921–5928, 2016.

587 [12] B. Schrader. *Infrared and Raman Spectroscopy: Methods and Applications.* John
588 Wiley & Sons Incorporated, Berlin, first ed. edition, 2008.

589 [13] T. Langner, A. Rietig, and J. Acker. Raman spectroscopic determination of the
590 degree of dissociation of nitric acid in binary and ternary mixtures with HF and
591 H_2SiF_6. *J. Raman Spectrosc.*, 51(2):366–372, 2020.

592 [14] D. Fraenkel. Structure and ionization of sulfuric acid in water. *New J. Chem.*,
593 39(7):5124–5136, 2015.

594 [15] W. W. Rudolph. Raman-spectroscopic measurements of the first dissociation con-
595 stant of aqueous phosphoric acid solution from 5 to 301 °C. *Journal of Solution*
596 *Chemistry*, 41(4):630–645, 2012.

597 [16] M. A. Elbagermi, A. I. Alajtal, H. G. M. Edwards, G. H. Azimi, K. D. Verma, and
598 I. J. Scowen. Raman spectroscopic and potentiometric studies of acidity level and
599 dissociation of citric acid in aqueous solution. *J. Appl. Chem. Sci. Int.*, 2(1):1–11,
600 2015.

601 [17] J. Huguenin, S. Ould Saad Hamady, and P. Bourson. Monitoring deprotonation of
602 gallic acid by Raman spectroscopy. *J. Raman Spectrosc.*, 46(11):1062–1066, 2015.

603 [18] H. Alatalo, J. Kohonen, H. Qu, H. Hatakka, S-P. Reinikainen, M. Louhi-Kultanen,
604 and J. Kallas. In-line monitoring of reactive crystallization process based on ATR-
605 FTIR and Raman spectroscopy. *J. Chemom.*, 22(11-12):644–652, 2008.

606 [19] T. D. Nguyen Hong, M. Jouan, N. Quy Dao, M. Bouraly, and F. Mantisi. Coupling of
607 high-performance liquid chromatography with Raman spectrometry. *J. Chromatogr.*
608 *A*, 743(2):323–327, 1996.

609 [20] F. Feidl, S. Garbellini, S. Vogg, M. Sokolov, J. Souquet, H. Broly, A. Butté, and
610 M. Morbidelli. A new flow cell and chemometric protocol for implementing in-line
611 Raman spectroscopy in chromatography. *Biotechnol. Prog.*, 35(5):e2847, 2019.

612 [21] K. S. Booksh. Chemometric methods in process analysis. In Robert A. Meyers,

editor, *Encyclopedia of Analytical Chemistry*, volume 71. John Wiley & Sons, Ltd, Chichester, UK, 2006.

[22] N. Kumar, A. Bansal, G. S. Sarma, and R. K. Rawal. Chemometrics tools used in analytical chemistry: An overview. *Talanta*, 123:186–199, 2014.

[23] A. Echtermeyer, C. Marks, A. Mitsos, and J. Viell. Inline Raman spectroscopy and Indirect Hard Modeling for concentration monitoring of dissociated acid species. *Appl. Spectrosc.*, 75(5):506–519, 2020.

[24] F. Alsmeyer, H-J. Koß, and W. Marquardt. Indirect spectral hard modeling for the analysis of reactive and interacting mixtures. *Appl. spectrosc.*, 58(8):975–985, 2004.

[25] E. Kriesten, D. Mayer, F. Alsmeyer, C. B. Minnich, L. Greiner, and W. Marquardt. Identification of unknown pure component spectra by Indirect Hard Modeling. *Chemom. Intell. Lab. Syst.*, 93(2):108–119, 2008.

[26] S. Wold, M. Sjöström, and L. Eriksson. Pls-regression: A basic tool of chemometrics. *Chemom. Intell. Lab. Syst.*, 58(2):109–130, 2001.

[27] Brian G Cox. *Acids and bases: Solvent effects on acid-base strength*. Oxford University Press, Oxford, UK, 2013.

[28] Adrien Albert and E.P. Serjeant. *The determination of ionization constants: A laboratory manual*. Chapman and Hall, New York, USA, 2012.

[29] Purolite. Chromalite^{TM} PCG1200C: RPC Macroporous adsorbent: Product data sheet.

[30] L. F. Kaven, H. J. M. Wolff, L. Wille, M. Wessling, A. Mitsos, and J. Viell. In-line monitoring of microgel synthesis: Flow versus batch reactor. *Org. Process Res. Dev.*, 25(9):2039–2051, 2021.

[31] H. Schmidt-Traub, M. Schulte, and A. Seidel-Morgenstern, editors. *Preparative Chromatography*. Wiley-VCH, Weinheim, third edition, 2020.

[32] O. Redlich and D. L. Peterson. A useful adsorption isotherm. *J. Phys. Chem.*, 63(6):1024, 1959.

[33] G. Guiochon, A. Felinger, D. G. Shirazi, and A. M. Katti. *Fundamentals of preparative and nonlinear chromatography*. Elsevier Academic Press, Amsterdam and Boston and Heidelberg and London and New York and Oxford and Paris and San Diego and San Francisco and Singapore and Sydney and Tokyo, second edition, 2006.

[34] Inc. Kaiser Optical Systems. Technical note 1250: Immersion optic for reaction monitoring: Technical report, 2006.

[35] O. Walz, M. Marks, J. Viell, and A. Mitsos. Systematic approach for modeling reaction networks involving equilibrium and kinetically-limited reaction steps. *Comput. Chem. Eng.*, 98:143–153, 2017.

[36] H.I. Moe, S. Hauan, K.M. Lien, and T. Hertzberg. Dynamic model of a system with phase- and reaction equilibrium. *Comput. Chem. Eng.*, 19:513–518, 1995. European Symposium on Computer Aided Process Engineering.

[37] J. Schell, E. Zars, C. Chicone, and R. Glaser. Simultaneous determination of all species concentrations in multiequilibria for aqueous solutions of dihydrogen phosphate considering debye–hückel theory. *J. Chem. Eng. Data*, 63(6):2151–2161, 2018.

[38] W. M. Haynes, D. R. Lide, and T. J. Bruno, editors. *CRC Handbook of Chemistry and Physics*. CRC Press, 2014.

[39] A. H. Truesdell and B. F. Jones. WATEQ, a computer program for calculating chemical equilibria of natural waters. *J. Res. US Geol. Surv.*, 2(2):233–248, 1974.

[40] Dale/DPP Prentice. *Thermodynamic modelling of ultra-long-term durability of cementitious binders for waste immobilisation.* PhD thesis, University of Sheffield, 2018.

[41] Walter Jay Hamer. Theoretical mean activity coefficients of strong electrolytes in aqueous solutions from 0 to 100 °C. *Natl. Stand. Ref. Data Syst.*, 1968.

[42] D. L. Parkhurst. Ion-association models and mean activity coefficients of various salts. In Daniel C. Melchior, editor, *Chemical modeling of aqueous systems*, volume 416 of *ACS Symposium Series*, pages 30–43. American Chem. Soc, Washington, 1990.

[43] W. Kessler. *Multivariate Datenanalyse für die Pharma-, Bio- und Prozessanalytik: Ein Lehrbuch.* Wiley-VCH, Weinheim, first edition, 2008.

[44] MATLAB. *Version 9.2.0 (R2017a).* The MathWorks Inc., Natick, Massachusetts, USA, 2018.

[45] K. de Gussem, J. de Gelder, P. Vandenabeele, and L. Moens. The biodata toolbox for MATLAB. *Chemom. Intell. Lab. Syst.*, 95(1):49–52, 2009.

[46] S. Kucheryavskiy. MATLAB toolbox for multivariate data analysis, 2016.

[47] W. R. Fenner, H. A. Hyatt, J. M. Kellam, and S. P. S. Porto. Raman cross section of some simple gases. *J. Opt. Soc. Am.*, 63(1):73–77, 1973.

[48] PEAXACT. *Version 5.3 – 5.4.* S-PACT GmbH, Aachen, Germany, 2022.

[49] E. Kriesten, F. Alsmeyer, A. Bardow, and W. Marquardt. Fully automated Indirect Hard Modeling of mixture spectra. *Chemom. Intell. Lab. Syst.*, 91(2):181–193, 2008.

[50] J-P. Conzen. *Multivariate Kalibration: Ein praktischer Leitfaden zur Methodenentwicklung in der quantitativen Analytik.* Bruker Optik, Ettlingen, fourth ed. edition, 2005.

[51] E. Desimoni and B. Brunetti. About estimating the limit of detection by the signal to noise approach. *Pharm. Anal. Acta*, 6(4):355–359, 2015.

Investigation of the elution behavior of dissociating itaconic acid on a hydrophobic polymeric adsorbent using in-line Raman spectroscopy

Andreas Biselli[1], Alexander Echtermeyer[2], Rafael Reifsteck[1], Peter Materla[1], Alexander Mitsos[2,3,4], Jörn Viell[2], Andreas Jupke[1]

[1]Fluid Process Engineering (AVT.FVT), RWTH Aachen University, 52074 Aachen, Germany
[2]Process Systems Engineering (AVT.SVT), RWTH Aachen University, 52074 Aachen, Germany
[3]JARA-ENERGY, 52062 Aachen, Germany
[4]Energy Systems Engineering (IEK-10), Forschungszentrum Jülich, 52425 Jülich, Germany

Supplementary material

Equation system for calculation of compositional data

A natural representation of the required model would be a differential-algebraic equation system [1, 2]. For historical reasons and consistency with our other simulation models, we approximate the system as a system of ordinary differential equations (Equations S1 – S10), assuming an arbitrary but thermodynamically consistent kinetic model [3, 4]. This is solved in Matlab R2021a (Mathworks, Massachusetts, USA) using the solver ode15s with an absolute tolerance of 10^{-12} and a relative tolerance of 10^{-6}.

$$\frac{\mathrm{d}c_{\mathrm{IAH_2}}}{\mathrm{d}t} = k_{\mathrm{a1,b}} \cdot a_{\mathrm{IAH^-}} \cdot a_{\mathrm{H_3O^+}} - k_{\mathrm{a1,f}} \cdot a_{\mathrm{IAH_2}} \cdot a_{\mathrm{H_2O}} \tag{S1}$$

$$\begin{aligned}\frac{\mathrm{d}c_{\mathrm{IAH^-}}}{\mathrm{d}t} = {} & k_{\mathrm{a1,f}} \cdot a_{\mathrm{IAH_2}} \cdot a_{\mathrm{H_2O}} - k_{\mathrm{a1,b}} \cdot a_{\mathrm{IAH^-}} \cdot a_{\mathrm{H_3O^+}} \\ & - k_{\mathrm{a2,f}} \cdot a_{\mathrm{IAH^-}} \cdot a_{\mathrm{H_2O}} + k_{\mathrm{a2,b}} \cdot a_{\mathrm{IA^{2-}}} \cdot a_{\mathrm{H_3O^+}}\end{aligned} \tag{S2}$$

$$\frac{\mathrm{d}c_{\mathrm{IA^{2-}}}}{\mathrm{d}t} = k_{\mathrm{a2,f}} \cdot a_{\mathrm{IAH^-}} \cdot a_{\mathrm{H_2O}} - k_{\mathrm{a2,b}} \cdot a_{\mathrm{IA^{2-}}} \cdot a_{\mathrm{H_3O^+}} \tag{S3}$$

$$\begin{aligned}\frac{\mathrm{d}c_{\mathrm{H_2O}}}{\mathrm{d}t} = {} & 2 \cdot k_{\mathrm{H_2O,b}} \cdot a_{\mathrm{H_3O^+}} \cdot a_{\mathrm{OH^-}} - 2 \cdot k_{\mathrm{H_2O,f}} \cdot a_{\mathrm{H_2O}} \cdot a_{\mathrm{H_2O}} \\ & + k_{\mathrm{a1,b}} \cdot a_{\mathrm{IAH^-}} \cdot a_{\mathrm{H_3O^+}} - k_{\mathrm{a1,f}} \cdot a_{\mathrm{IAH_2}} \cdot a_{\mathrm{H_2O}} \\ & + k_{\mathrm{a2,b}} \cdot a_{\mathrm{IA^{2-}}} \cdot a_{\mathrm{H_3O^+}} - k_{\mathrm{a2,f}} \cdot a_{\mathrm{IAH^-}} \cdot a_{\mathrm{H_2O}} \\ & + k_{\mathrm{HCl,b}} \cdot a_{\mathrm{H_3O^+}} \cdot a_{\mathrm{Cl^-}} - k_{\mathrm{HCl,f}} \cdot a_{\mathrm{HCl}} \cdot a_{\mathrm{H_2O}}\end{aligned} \tag{S4}$$

$$\begin{aligned}\frac{\mathrm{d}c_{\mathrm{H_3O^+}}}{\mathrm{d}t} = {} & k_{\mathrm{a1,f}} \cdot a_{\mathrm{IAH_2}} \cdot a_{\mathrm{H_2O}} - k_{\mathrm{a1,b}} \cdot a_{\mathrm{IAH^-}} \cdot a_{\mathrm{H_3O^+}} \\ & + k_{\mathrm{a2,f}} \cdot a_{\mathrm{IAH^-}} \cdot a_{\mathrm{H_2O}} - k_{\mathrm{a2,b}} \cdot a_{\mathrm{IA^{2-}}} \cdot a_{\mathrm{H_3O^+}} \\ & + k_{\mathrm{H_2O,f}} \cdot a_{\mathrm{H_2O}} \cdot a_{\mathrm{H_2O}} - k_{\mathrm{H_2O,b}} \cdot a_{\mathrm{H_3O^+}} \cdot a_{\mathrm{OH^-}} \\ & + k_{\mathrm{HCl,f}} \cdot a_{\mathrm{HCl}} \cdot a_{\mathrm{H_2O}} - k_{\mathrm{HCl,b}} \cdot a_{\mathrm{H_3O^+}} \cdot a_{\mathrm{Cl^-}}\end{aligned} \tag{S5}$$

$$\begin{aligned}\frac{\mathrm{d}c_{\mathrm{OH^-}}}{\mathrm{d}t} = {} & k_{\mathrm{H_2O,f}} \cdot a_{\mathrm{H_2O}} \cdot a_{\mathrm{H_2O}} - k_{\mathrm{H_2O,b}} \cdot a_{\mathrm{OH^-}} \cdot a_{\mathrm{H_3O^+}} \\ & + k_{\mathrm{NaOH,f}} \cdot a_{\mathrm{NaOH}} - k_{\mathrm{NaOH,b}} \cdot a_{\mathrm{Na^+}} \cdot a_{\mathrm{OH^-}}\end{aligned} \tag{S6}$$

$$\frac{\mathrm{d}c_{\mathrm{HCl}}}{\mathrm{d}t} = k_{\mathrm{HCl,b}} \cdot a_{\mathrm{H_3O^+}} \cdot a_{\mathrm{Cl^-}} - k_{\mathrm{HCl,f}} \cdot a_{\mathrm{HCl}} \cdot a_{\mathrm{H2O}} \tag{S7}$$

$$\frac{\mathrm{d}c_{\mathrm{Cl^-}}}{\mathrm{d}t} = k_{\mathrm{HCl,f}} \cdot a_{\mathrm{HCl}} \cdot a_{\mathrm{H2O}} - k_{\mathrm{HCl,b}} \cdot a_{\mathrm{H_3O^+}} \cdot a_{\mathrm{Cl^-}} \tag{S8}$$

$$\frac{\mathrm{d}c_{\mathrm{NaOH}}}{\mathrm{d}t} = k_{\mathrm{NaOH,b}} \cdot a_{\mathrm{Na^+}} \cdot a_{\mathrm{OH^-}} - k_{\mathrm{NaOH,f}} \cdot a_{\mathrm{NaOH}} \tag{S9}$$

$$\frac{\mathrm{d}c_{\mathrm{Na^+}}}{\mathrm{d}t} = k_{\mathrm{NaOH,f}} \cdot a_{\mathrm{NaOH}} - k_{\mathrm{NaOH,b}} \cdot a_{\mathrm{Na^+}} \cdot a_{\mathrm{OH^-}} \tag{S10}$$

Thereby, a_i of respective components is defined as

$$a_i = c_i \cdot \gamma_i, \tag{S11}$$

with γ_i representing the respective activity coefficient. K_i of respective components is defined as

$$K_i = \frac{k_{i,\mathrm{f}}}{k_{i,\mathrm{b}}}, \tag{S12}$$

with $k_{i,\mathrm{f}}$ and $k_{i,\mathrm{b}}$ representing the forward and backward reaction rates, respectively. Since only dissociation equilibria are evaluated, the forward reaction rate $k_{i,\mathrm{f}}$ is set to 100 (an arbitrary

value which is high enough) [3] and the corresponding backward reaction rate $k_{i,\mathrm{b}}$ is calculated according to equation S12 to ensure thermodynamic consistency.

IHM: Construction and calibration results

The five pure component models (PCMs) of IAH_2, IAH^-, IA^{2-}, water, and PTFE that are constructed by IHM and CHM are shown in Figure S1 (**a**) – (**e**). The most characteristic difference between the PCMs of the IA species is the intensity of the pseudo-Voigt profile modeling the carbonyl stretching mode $\nu_{s,\mathrm{C=O}}$ at 1700 cm^{-1}. It decreases in relation to the carbon-carbon double bond stretching mode $\nu_{\mathrm{C=C}}$ at 1643 cm^{-1} for increased dissociation.

The mixture hard model (HM) combining the five PCMs with a linear baseline model is fitted to a representative mixture spectrum and is shown in Figure S2 (**f**) for the case of TdJ-based composition calculation. It becomes apparent that PTFE exhibits the most prominent signals in the evaluated spectral range and therefore requires the respective signal compensation by inclusion of a PTFE PCM. The Raman bands of the IA species largely overlap with the Raman bands of water in the spectral range of $\tilde{\nu}$ = 1500 – 1800 cm^{-1}, but can be clearly resolved and fitted by the HM. The quality of the spectral fit is reflected by the fitting residuals displayed in Figure S2 (**g**). As the residuals are low and uniformly distributed, we conclude that the HM represents the spectral data very well.

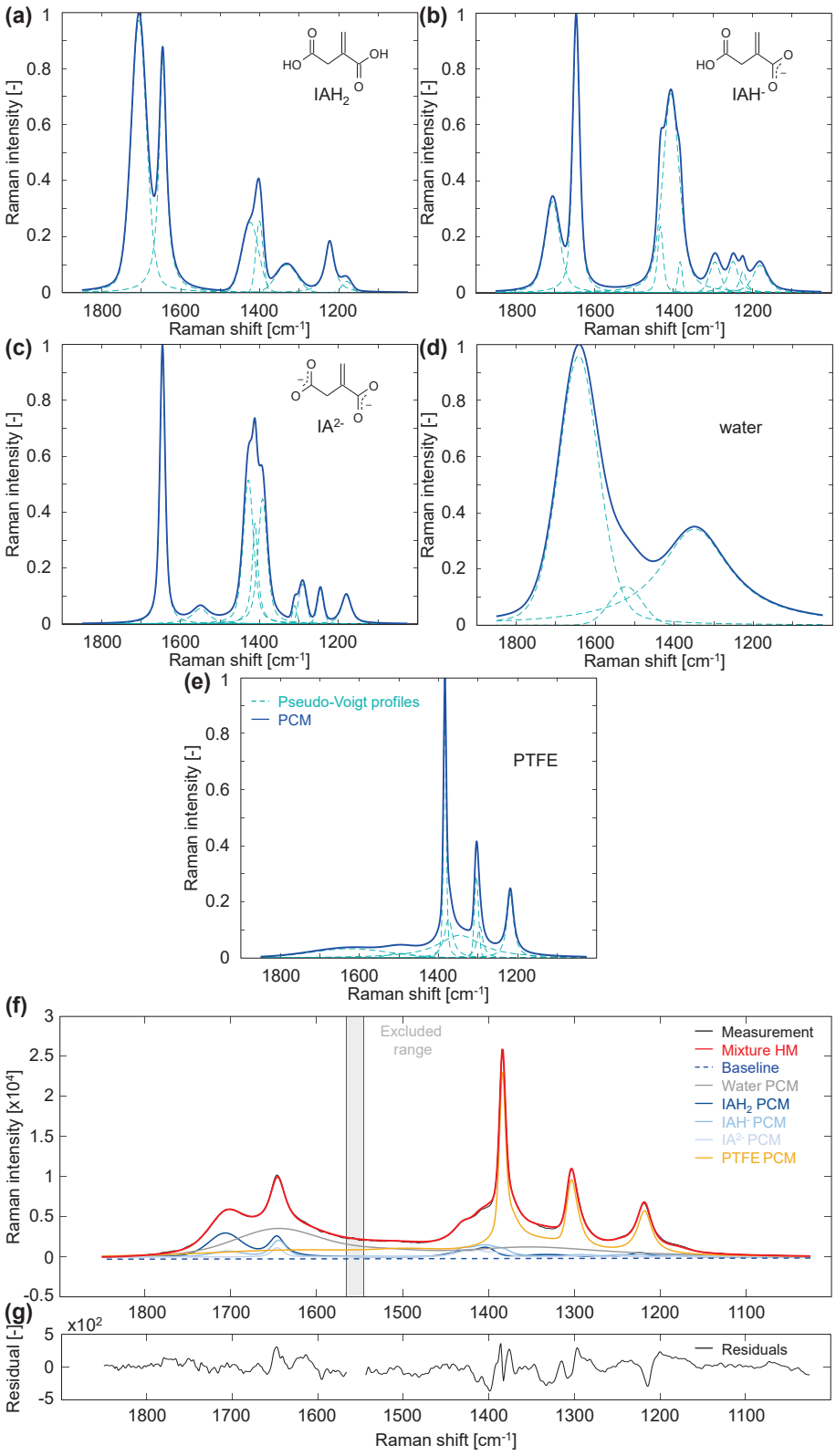

Figure S1: Assumption of ideal thermodynamics: PCMs of IAH_2 (**a**), IAH^- (**b**), IA^{2-} (**c**), water (**d**), and PTFE (**e**) that are combined with a linear baseline model to form the mixture HM, which is fitted to a representative in-line Raman spectrum (**f**). The residuals of the HM fit are displayed in (**g**).

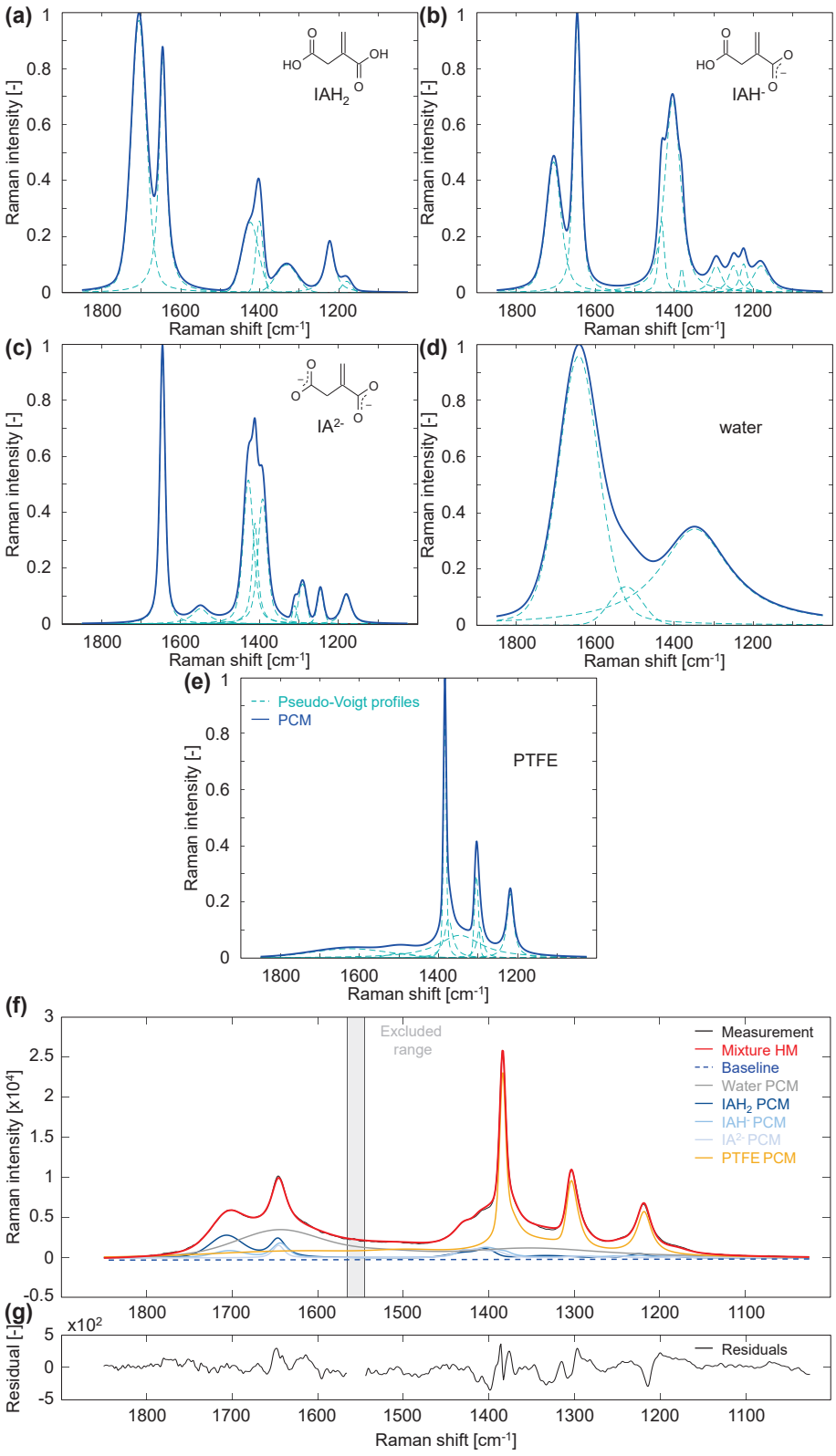

Figure S2: Assumption of non-ideal thermodynamics (TdJ): PCMs of IAH_2 (**a**), IAH^- (**b**), IA^{2-} (**c**), water (**d**), and PTFE (**e**) that are combined with a linear baseline model to form the mixture HM, which is fitted to a representative in-line Raman spectrum (**f**). The residuals of the HM fit are displayed in (**g**).

The parity plots with figures of merit for the mixture HM calibrated on the basis of ideality assumptions are shown in Figure S3 (**a**) – (**d**), whereas the same information is shown in Figure S4 (**a**) – (**d**) for the HM calibrated subject to considered activity coefficients. It becomes apparent that in both figures all data points scatter randomly around the unity line, indicating the absence of systematic errors. For all four species in both HMs, the values of R^2 are close to one symbolizing that the models represent the variations in the underlying calibration data very well. As the values for $RMSEC$ and $RMSECV$ are small compared to the overall concentration range applied for calibration, we conclude that both calibrations provide accurate results. Moreover, for both calibrations, the values of $RMSEC$ and $RMSECV$ are similar or very close to each other, which confirms the selection of a sufficiently large calibration data set. As the values for LOD are in the same order of magnitude or even much smaller than the calibration errors, we conclude that the chemometric method is sufficiently sensitive and feasible for application in the desired process monitoring. A direct comparision of the calibration results of the two HMs reveals only minor differences especially for the dissociated IA species IAH^- and IA^{2-}. A certain improvement in their calibration accuracy is expected as the consideration of activity coefficients during calculation of the acid species dissociation mostly affects IAH^- and IA^{2-} concentrations and is not so much reflected by changes in water and associated acid species content.

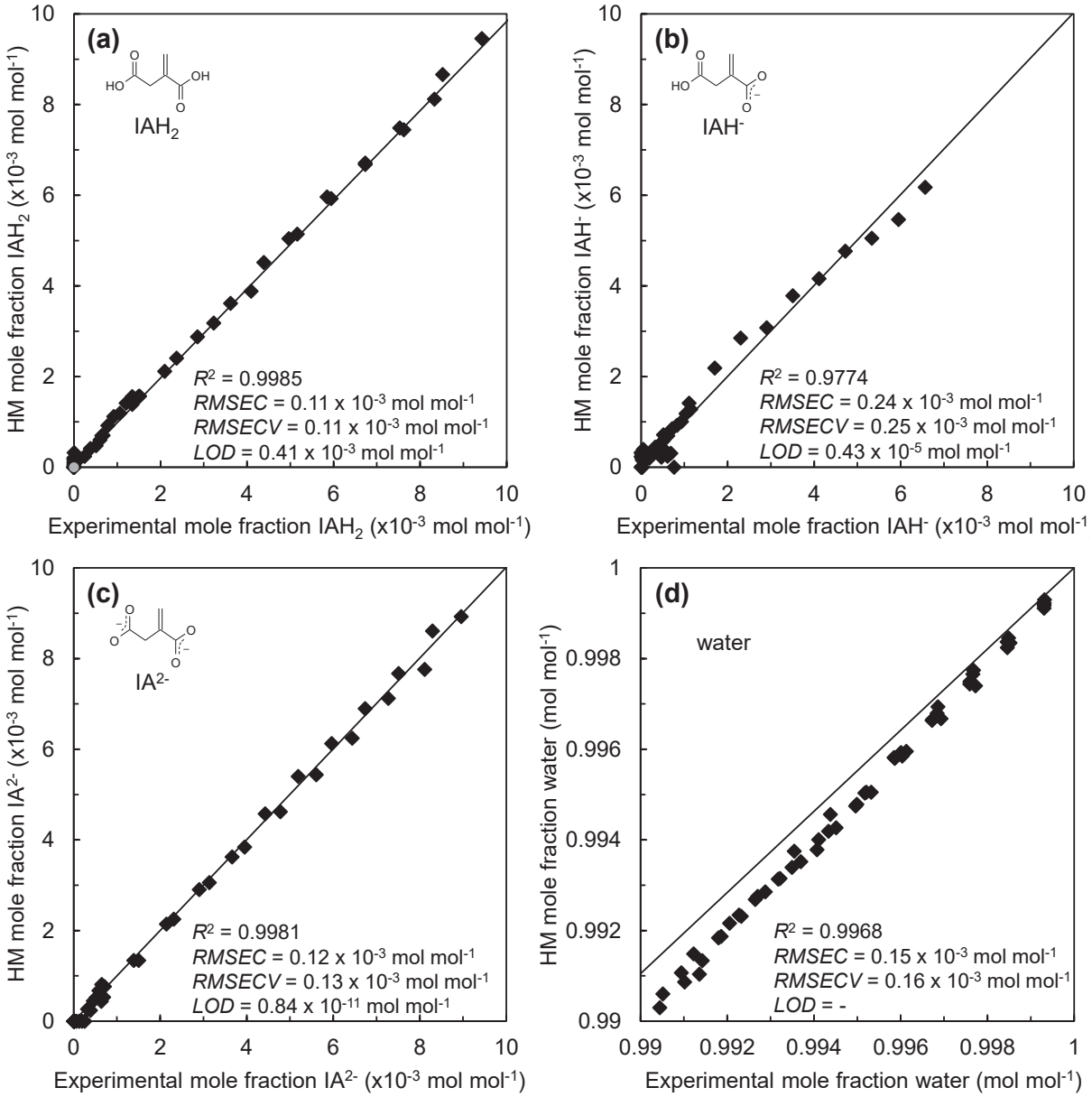

Figure S3: Parity plots with figures of merit for HM calibration of the species IAH_2 (**a**), IAH^- (**b**), IA^{2-} (**c**), and water (**d**) on the basis of composition data from calculations assuming ideal dissociation conditions.

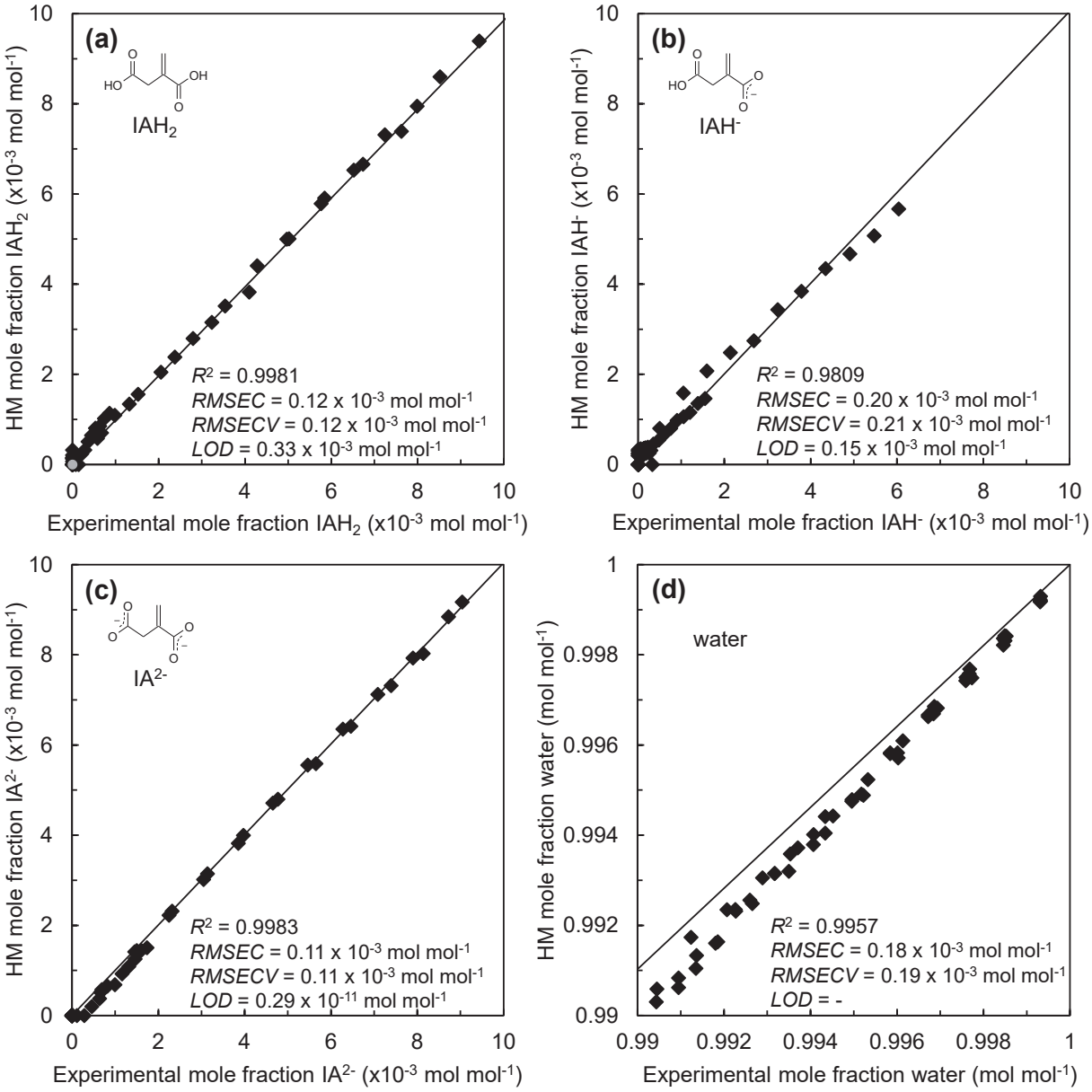

Figure S4: Parity plots with figures of merit for HM calibration of the species IAH_2 (**a**), IAH^- (**b**), IA^{2-} (**c**), and water (**d**) on the basis of composition data using a Truesdell-Jones equation for activity coefficient calculation of the non-ideal dissociation conditions.

Flow-through cell

Figure S5 (a) – (c) depicts the custom-made flow cell utilized for in-line Raman spectroscopy measurements. The material of the cell is PTFE. The capillary within the flow-cell had an inner diameter of 0.8 mm. The length of the capillary is approximately 20 mm.

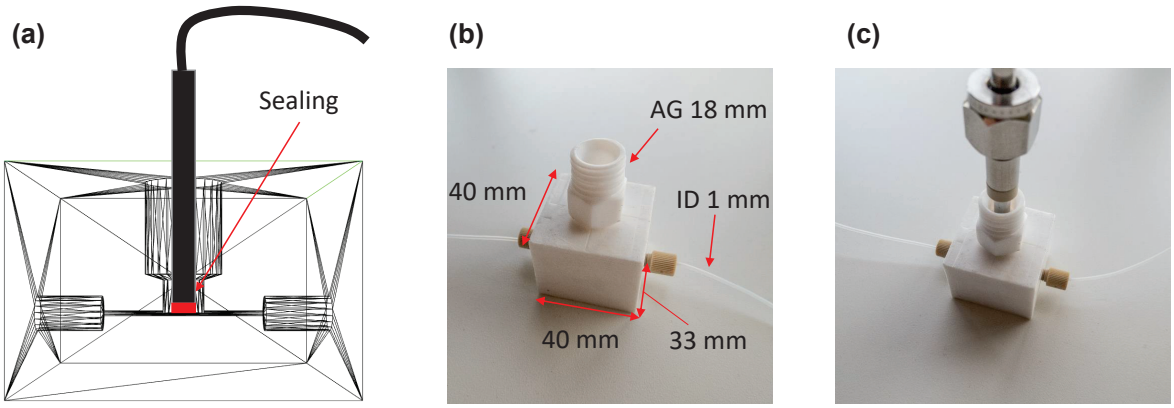

Figure S5: (a): Schematic illustration of the custom-made flow-through cell made of PTFE for in-line Raman spectroscopy measurements. (b) and (c): Pictures of flow-through cell.

Pulse experiments with 95% uncertainty included

Figures S6 - S8 show the pulse experiments at feed pH values of 2, 4.5, and 8, as depicted in the Figures 5 (a), (c), and (e), supplemented by respective 95% uncertainties of the species concentrations based on the assumption of ideal thermodynamics. It becomes apparent that low concentrations within the pulse experiments lie within the 95% uncertainty intervals. Thus, the limited significance of these values should be considered.

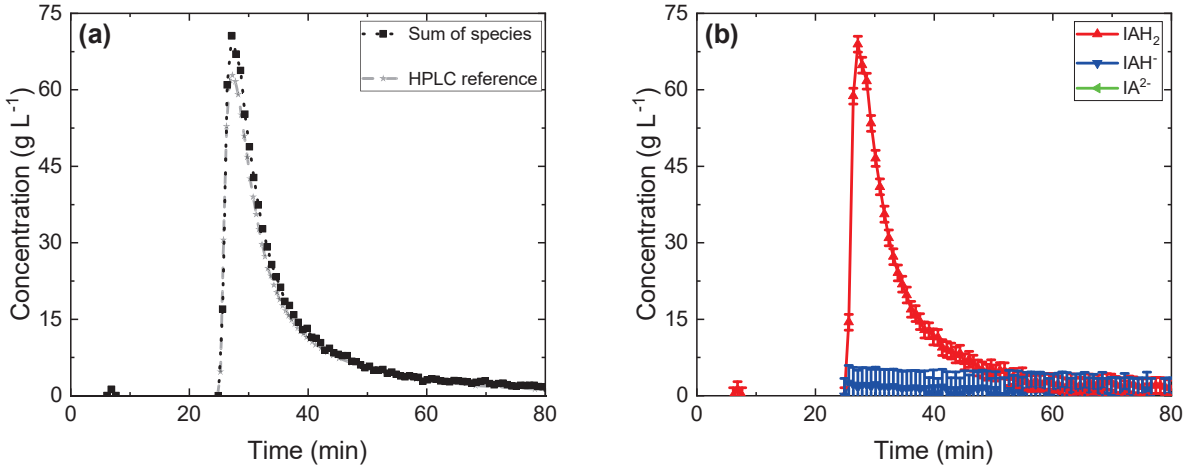

Figure S6: Pulse experiment at a pH value of 2: (a) Chromatogram of the pulse experiment including IA concentrations determined via HPLC as well as total IA concentrations determined as sum of species measured via in-line Raman spectroscopy. (b) Individual IA species concentrations including respective uncertainties (95%) in species concentrations.

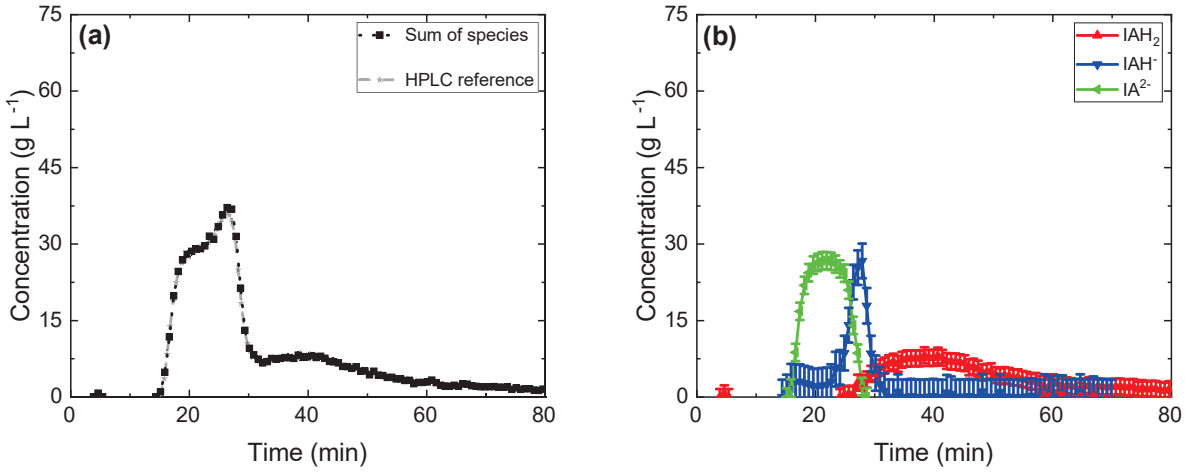

Figure S7: Pulse experiment at a pH value of 4.5: (a) Chromatogram of the pulse experiment including IA concentrations determined via HPLC as well as total IA concentrations determined as sum of species measured via in-line Raman spectroscopy. (b) Individual IA species concentrations including respective uncertainties (95%) in species concentrations.

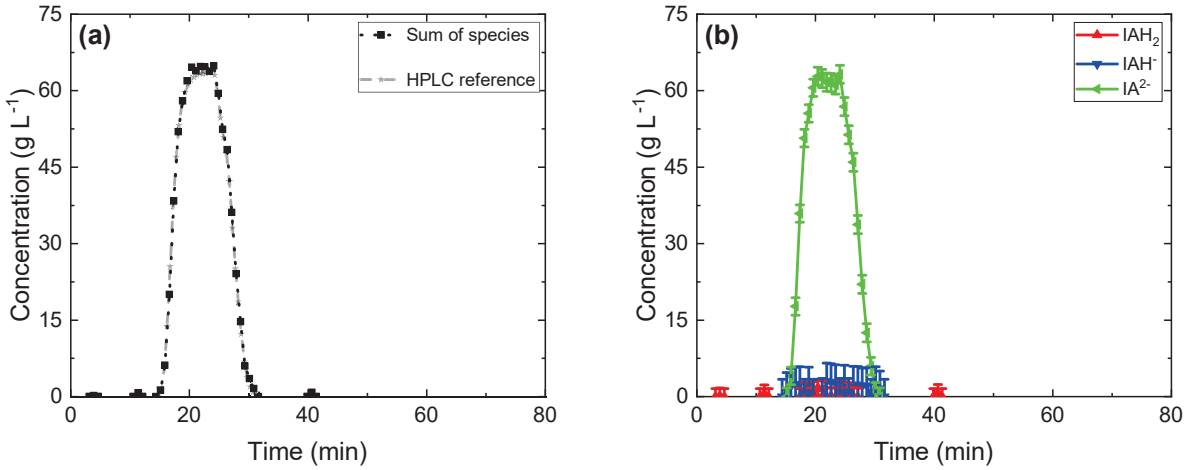

Figure S8: Pulse experiment at a pH value of 8: (a) Chromatogram of the pulse experiment including IA concentrations determined via HPLC as well as total IA concentrations determined as sum of species measured via in-line Raman spectroscopy. (b) Individual IA species concentrations including respective uncertainties (95%) in species concentrations.

References

[1] O. Walz, M. Marks, J. Viell, and A. Mitsos. Systematic approach for modeling reaction networks involving equilibrium and kinetically-limited reaction steps. *Comput. Chem. Eng.*, 98:143–153, 2017.

[2] H.I. Moe, S. Hauan, K.M. Lien, and T. Hertzberg. Dynamic model of a system with phase- and reaction equilibrium. *Comput. Chem. Eng.*, 19:513–518, 1995. European Symposium on Computer Aided Process Engineering.

[3] J. Schell, E. Zars, C. Chicone, and R. Glaser. Simultaneous determination of all species concentrations in multiequilibria for aqueous solutions of dihydrogen phosphate considering debye–hückel theory. *J. Chem. Eng. Data*, 63(6):2151–2161, 2018.

[4] F. Horn and R. Jackson. General mass action kinetics. *Archive for Rational Mechanics and Analysis*, pages 81–116, 1972.